INFLUENCE OF NEBULIN ON THE ASSEMBLY MECHANICS OF DESMIN

An Undergraduate Research Scholars Thesis

by

MARC ADRIAN CARAGEA

Submitted to Honors and Undergraduate Research
Texas A&M University
In partial fulfillment of the requirements for the designation as

UNDERGRADUATE RESEARCH SCHOLAR

Approved by
Research Adviser: Gloria M. Conover, Ph.D.

May 2014

Major: Biomedical Sciences

TABLE OF CONTENTS

ABSTRACT

Influence of Nebulin on the Assembly Mechanics of Desmin. (May 2014)

Marc Adrian Caragea
Department of Biochemistry & Biophysics
Texas A&M University

Research Advisor: Gloria M. Conover, Ph.D.
Department of Biochemistry & Biophysics

Desmin intermediate filaments (DIFs) bind to nebulin, forming a direct link between the intermediate filament (IF) cytoskeletal network and the Z-discs of myofibrils in muscle cells. As the main IF in muscles, desmin is important for the sarcomeres functional and structural organization. This structural alignment of myofibrils is responsible for maintaining the contractile apparatus, providing cellular stability and force transmission throughout the muscle system. The DIF mutant, E245D, is a missense mutation resulting in the substitution of aspartic acid for glutamic acid in the coil 1B region of desmin, a major binding site for nebulin. This DIF mutation is linked to desminopathy in humans, which is a debilitating familial disease associated with restrictive cardiomyopathies and progressive skeletal muscle weakness of the upper and lower extremities. This study aims to gain insight on the molecular mechanisms involved in desmin IF assembly when influenced by its association with nebulin. The E245D mutation was chosen as it maps in the high-affinity nebulin-binding 1B region of desmin. We will employ atomic force microscopy (AFM) to analyze the lengths and elasticity of DIFs using recombinantly generated human desmin and nebulin proteins.

ACKNOWLEDGMENTS

This research is funded by SDG-AHA grant 2110057 to G.M.C. The authors are grateful for the assistance from Daniel A. Hernandez for providing protein purifications for experiments and Dr. Wilson Serem for expert technical advice on the AFM instrument.

NOMENCLATURE

AFM	Atomic Force Microscope
C	Celsius
DIF	Desmin Intermediate Filament
E	Young's Modulus
E245D	Glutamate 245 Aspartate
GPa	Gigapascal
IF	Intermediate Filament
kDa	Kilodalton
KO	Knock-Out
µm	micrometer
min	minuet
MT	Microtubule
MWCO	Molecular weight cut-off
QNM	Quantitative nanomechanical property mapping
ULF	Unit-Length Filament
WT	Wild Type
3D	Three-Dimensional

CHAPTER I

INTRODUCTION

The cytoskeleton, a network of highly cross-linked filaments located within cells, extends throughout the cytoplasm, organizing internal organelles and orchestrating many cellular activities. One of the primary functions of the cytoskeleton is to maintain cell shape by providing mechanical support and resistance to cellular stress. The cytoskeleton of eukaryotic cells is composed of three main structural proteins: microtubules (MTs), actin filaments, and intermediate filaments (IFs), with the latter of the three being the primary focus of our study. MTs, the largest of the three, are 25 nm thick dimers made of hollow columns composed of α-tubulin and β-tubulin, and contribute to maintain cell shape by resisting compression. With a diameter of approximately 6-7 nm, actin filaments, also known as microfilaments, are the thinnest of the three cytoskeletal proteins. Actin filaments, composed of globular protein actin, are built by a coiled double chain of actin subunits. Actin filaments are relatively flexible tension-bearing proteins, helping to maintain cell shape by forming a three-dimensional (3D) network. In contrast to actin and MTs, all IFs are 8-12 nm thick non-polar filaments that form supercoiled structures via their α-helical central coiled-coil domain. IFs are comprised of many different types of proteins in a broad range of tissues, but like actin filaments, they are also tension-bearing fibers. Of the three, IFs are the most flexible filaments, play cytoprotective roles against cellular stress, and are important in scaffolding multi-protein complexes. Our study focuses on IF mutations, which have been known to cause over 80 distinct human diseases [1], highlighting the importance in cellular function of this superfamily of cytoskeletal proteins.

One of the most abundant IFs in muscle tissue is desmin. Desmin interlinks and aligns myofibrils composed of serially connected sarcomeres. The sarcomere, the basic unit of a muscle, is composed of interdigitating actin and myosin filaments that are bordered by Z-discs. During muscle contraction, actin and myosin filaments slide past one another, decreasing the distance between adjacent Z-discs, thereby changing the length of the entire muscle organ. Desmin is essential for the structural stability of the sarcomere in myocytes because it forms a 3D scaffold, connecting series of myofibrils to the plasma membrane and the nuclear envelope [2]. Desmin directly binds to the actin-binding protein nebulin, forming a link between the IF network and sarcomeres at the Z-discs [3]. Interestingly, nebulin knock-out (KO) skeletal muscle exhibits highly misaligned myofibrils, probably due to the decrease of desmin localization at the Z-discs [4]. The correct alignment of myofibrils provided by the desmin network is paramount for force transmission throughout the myofibers [5]. Clinical manifestations caused by the disruption of the desmin cytoskeleton scaffold are described in humans as skeletal and cardiac myopathies characterized by progressive bilateral weakness of the extremities that eventually leads to wheelchair dependence [6, 7]. Desminopathy, also known as desmin-related myopathy, is one such example. It is a myofibril myopathy most commonly associated with *de novo* mutations in the *DES* gene, with autosomal dominant or autosomal recessive inheritance [7].

Desmin is a 53-kDa protein comprised of 476 amino acids that forms a coiled-coil dimer via its central α-helical domain. The dimer is separated by non-helical linkers into three consecutive helical segments (1A, 1B, 2). A remarkable property of desmin intermediate filaments (DIFs), like that of other IF proteins, is that they self-assemble *in vitro* by antiparallel lateral interactions of dimers under high ionic strength [8]. This dimer-dimer interaction results in unit-length

filaments (ULFs) approximately 65 nm in length, which anneal longitudinally to form mature filaments (Fig. 11). The filaments crosslink, integrating to form a dense, yet highly flexible, biopolymer network [8, 9]. Surprisingly, the mass-per-length composition of DIFs at two seconds, as compared to one hour after initiation of assembly, was found to be similar, with approximately 47 molecules per-cross section [8]. This finding highlights the speed and consistency of ULF formation throughout the DIF assembly process.

Mutations in desmin cause disease by preventing the formation of protein filaments at different stages of the filament assembly process, leading to the aggregation of desmin and other proteins [9, 10]. There are currently 45 disease-causing *DES* mutations, the majority of which are missense mutations occurring in the 2B segment [7]. The rate of disease progression and the age of onset vary, and are not correlated to the location of the mutation. Notably, the desmin Glu245Asp (E245D) is a single missense mutation resulting in the substitution of aspartic acid for glutamic acid in the coil 1B region of desmin that causes skeletal myopathies along with early on-set restrictive cardiomyopathy in humans. Interestingly, this mutant was shown to bind to the C-terminal of nebulin (modules 160-164) with high affinity [3]. Electron microscopy analysis of the mutant desmin E245D demonstrated that this mutant forms seemingly normal-looking filaments [9], indicating that other molecular defects such as an improper binding between mature desmin E245D filaments and binding partners may be responsible for the molecular phenotypes found in desmin-related myopathy patients [3]. In this study, we hypothesize that the ineffective binding between nebulin and the mutant desmin E245D will disturb filament lengths along with the mechanical properties of DIF networks.

Using a reconstitution biochemical approach coupled with atomic force microscopy (AFM), this study aims to gain a better understanding of the mechanical properties of desmin while bound to its muscle binding-partner nebulin. We assessed filament lengths of desmin WT and mutant E245D in the presence and absence of nebulin, 10 min after the initiation of assembly. In our studies, we used a scanning probe microscope (or AFM), which uses a tip or cantilever probe to scan the surface of immobilized desmin filaments. This technique renders an image that allows us measure filament lengths, providing the ability to assess changes in topology. This approach also allows us to determine how the topology and lengths of single desmin filaments were impacted by their association to nebulin at a nanoscale level. Additionally, we determined the overall stiffness and elasticity of the DIF networks formed in the presence and absence of nebulin. To do this, we employed a force-distance measurement to calculate the Young's modulus (E), also known as elastic modulus. E is a measurement of stiffness, which refers to the extent to which a material resists deformation in response to an applied force. A comparison of Young's modulus will quantify the influence of nebulin on dense glutaraldehyde-stabilized networks of WT and mutant desmin filaments. Collectively, our results are expected to yield novel mechanisms that could help explain how sarcomere proteins regulate desmin network mechanics, and to possibly help explain the defects found at the single molecular level for the pathogenesis of a class of desmin mutations linked to human desminopathy.

CHAPTER II

MATERIALS AND METHODS

Affinity purification of human WT and mutant desmin proteins from bacteria

Recombinant desmin proteins were induced in *E. coli* BL-21 at 37°C overnight and purified out of inclusion bodies from pDS5 untagged vector, followed by two ion exchange chromatography purification steps as previously described [11]. After 3 hour induction with 0.5 M IPTG, bacterial cells were resuspend in cold lysis buffer (100 mM NaH_2PO_4, 10 mM NaCl, 5 mM imidazole). The lysates were transferred to Dounce homogenizers (Sartorius, Germany), and 0.2% Triton X-100, 10% NP-40, and 10 mM $MgCl_2$ were added. Desmin was purified from inclusion bodies using Fast Flow diethylaminoethanol (DEAE) ion-exchange chromatography in column buffer (8 M Urea, 5 mM Tris-HCl, 1 mM EDTA, 0.1 EGTA, 1 mM DTT, pH 7.5). Bound proteins were eluted with a 0-0.3 M KCl salt gradient using a peristaltic pump (Bio-Rad) with the flow rate of 1.45 mL/min. Protein fractions were analyzed using SDS-PAGE and peak fractions were pooled based on gel appearance and concentration as determined by Bradford assays. To determine the fractions that contained high concentrations of protein, aloquats were chosen using the droplet test on parafilm. That is, the droplets for the samples containing the most protein turned form brownish-red to dark-blue. A second carboxymethly (CM)-Sepharose column was made in column buffer. After the Fast Flow CM-Sepharose column, peak fractions were identified by Bradford assay and by SDS-PAGE before storing. Fractions containing high and low amounts of protein were pooled, aliquoted in low-binding protein eppendorf tubes, rapidly snap-frozen in liquid nitrogen and stored at -80°C.

Affinity purification of recombinant nebulin M160 – 164

A recombinant nebulin protein fragment encompassing modules M160 – 164 with an N-terminal 6x Histidine tag was purified using the methods described in the QIAexpressionist protein purification manual (Qiagen). This particular nebulin fragment was chosen because it was reported to have the highest affinity binding site for desmin. Some modifications were introduced to optimize the protein yield as described next. A starter culture of *E. coli* BL-21 expressing human pET15b-Neb M160-164 was grown in Luria broth (LB) (1% NaCl, 0.5% yeast extract, and 1% tryptone) supplemented with 100 µg/µl ampicillin, overnight shaking with aeration at 37°C. After 24 hours, 20 mLs of the starter *E. coli* culture was added to 1 L of LB, supplemented with ampicillin and incubated further for approximately 2 hours at 37°C. After OD_{600} absorbance reading reached ~0.6, 1 mL 0.5 M IPTG (to obtain a final concentration of 0.5 mM IPTG) was added to 1 L of bacterial culture and incubated for 3 hours at 37°C. The bacterial cultures were centrifuged for 10 min at 5000 rpms and the pellets were stored overnight at -20°C. Samples were collected before and after IPTG addition for nebulin expression analysis by SDS-PAGE.

The day of the purification, bacterial pellets were weighed and lysis buffer (100 mM NaH_2PO_4, 10 mM NaCl, 5 mM imidazole) was added at a ratio of 2 mL per gram of weight on ice. An ULTRA tablet EDTA-free (Roche) protease inhibitor cocktail was dissolved in the lysis buffer prior to suspension (1 tablet per 10 mL). The pellets were dislodged from the centrifugation tube by repetitive pipetting in order make a homogenous lysate. Lysozyme (Sigma) was added to the lysis buffer at 1 mg/mL followed by 30 min incubation on ice. Next, each pellet was transferred to a dounce homogenizer to ensure lysis of bacterial cell walls. A final concentration of 1%

Triton X-100 was added to the pellets to aid with solubilization of insoluble proteins at 4°C, by gently rotating conicals containing the lysates. After 30 min, solubilized proteins were centrifuged at 10,000 rpm for 30 min to clarify lysates and other materials. Soluble protein samples were collected throughout the purifications steps to evaluate by SDS-PAGE.

The nickel Ni-NTA agarose beads (Qiagen) were rinsed in wash buffer (100 mM NaH_2PO_4, 10 mM NaCl, 10 mM imidazole, 20% Triton X-100) three times prior to addition to the cleared bacterial lysate. Tubes containing the lysate and Ni-NTA beads were incubated at 4°C rotating for 1 hour. After the incubation was completed, the beads were centrifuged for 1 min and the supernatant was removed and stored as 4°C. The supernatant contained the proteins that did not bind to the beads. The Ni-NTA beads were washed again and mixed with the supernatant to collect any remaining tagged protein left in the unbound fraction, followed by an overnight incubation on a rotating platform at 4°C.

The nebulin M160-164-Ni-NTA coupled beads were washed with 10 volumes of wash buffer four times. Protein bound beads were eluted using elution buffer (50 mM NaH_2PO_4, 300 mM NaCl, 250 mM imidazole) by incubating tubes at 4°C for 8 min followed by 1 min centrifugation in a table top centrifuge at 15000 rpm. Supernatants were saved on ice and the elution process was repeated four times. Elutions were also performed separately for overnight lysate bound beads. Samples were collected from each elution procedure and analyzed by SDS-PAGE. Based on the gel profile, nebulin fractions containing highest and cleanest protein were placed into a dialysis bag with MWCO of 8 kDa (Spectrum Laboratories, Rancho Dominguez, CA) and dialyzed overnight at 4° C in Tris-HCl dialysis buffer pH 8.4. After 2 hours, the buffer was

replaced, and the dialysis was set to stir overnight at 4°C. After the dialysis, a final concentration of 15% glycerol was added to the dialyzed human His-nebulin M160-164 protein and aliquots were snap-frozen in liquid nitrogen and stored at -80° C.

Assembly protocol for desmin precursors into filaments *in vitro*

Desmin filament precursors, as prepared above, were dialyzed out of 8 M urea using a step-wise dialysis protocol in a low ionic strength Tris-HCl based dialysis buffer (5mM Tris, 1mM EDTA, 0.1mM EGTA, 1mM DTT, pH 8.4). A dialysis bag containing the protein with MWCO of 8 kDa (Spectrum Laboratories, Rancho Dominguez, CA) was placed into 8 M urea (10 M Urea, Tris-HCl dialysis buffer, 1mM DTT, pH 8.4). The dialysis bag is permeable to urea but impermeable to the protein, so the urea is dialyzed out sequentially by a series of two-fold dilutions (8 M, 4 M, 2 M, and 1 M) at room temperature. During the last step, the protein is dialyzed overnight at 4° C in dialysis buffer without urea in a total volume of 600 mL.

Sample preparation for atomic force microscopy

To make soluble desmin precursors to assemble into filaments, desmin initially was dialyzed out of 8 M Urea in Tris-HCl dialysis buffer the day before, as described above. Figure 1 shows a flowchart outlining the steps used for the AFM sample preparations. For single filament measurements, proteins were diluted in Tris-HCl dialysis buffer and adjusted to an initial starting concentration of 0.1 g/L. Adjusting the initial concentration modulates the capacity to form networks. When dense desmin filament networks are needed for force measurements, rather than single filaments for length measurements, the concentrations are increased 10-fold, with and initial concentration of 1.0 g/L, resulting in a final concentration of 0.125 g/L. 10 μL of protein

was added to 2x low assembly buffer (2xAB) (10 mM NaCl, 4 mM Tris-HCl, pH 7.0) at a 1 to 1 molar ratio at 37°C for 10 min. The 2x AB at 37°C mimics the physiological buffer ionic strength and pH conditions that trigger IF proteins assembly, and is known to initiate the assembly process into elongated filament fibers and networks [11]. 10 µLs of the sample was removed and further diluted in 1xAB (5 mM NaCl, 2 mM Tris-HCl, pH 7.0) to a 1 to 1 molar ratio. 10 µL of the sample was removed and added to freshly prepared 0.25% glutaraldehyde vial at a 1 to 1 ratio to obtain a final concentration of 0.0125 g/L.

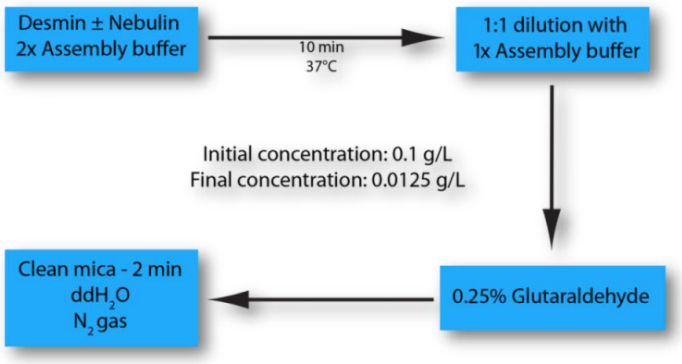

Figure 1: Atomic force microscopy protein sample preparation procedure. The flowchart lists the steps used to obtain single desmin filaments for AFM imaging. 10 µL of protein was transferred between each step, with 5 µL of diluted protein added to the mica surface. The procedure for obtaining dense filament networks is the same except for a 10-fold increase in protein concentration, with an initial concentration of 1.0 g/L and a final concentration of 0.125 g/L.

Glutaraldehyde is a biological fixative that stops filament elongation by crosslinking ULFs via covalent inter-subunit bonds. Next, 5 µL of the sample was removed and placed on freshly cleaved mica (TED PELLA, Redding, CA). All mica was cleaved using double sided tape in order to expose a clean and smooth surface. After 2 min of protein contact with the mica surface, unattached protein was washed off using ddH_2O and the sample was dried with N_2 gas. The undersurface of the mica (surface without protein) was labeled with permanent marker. Due to

the transparent properties of mica, the undersurface markings are visible to the high-resolution camera and serve as a guide for more efficient sample navigation.

Single desmin filament length acquisition and analysis

Protein samples for length measurements were scanned on mica by Bruker Dimension Icon AFM using PeakForce quantitative nanomechanical mapping (QNM) mode in air, tip model: TAP150A (Bruker). The AFM equipment configuration is illustrated in Figure 2. We employed a basic deflection-type set-up in which the laser beam, emitted by the diode, is reflected off the AFM tip and detected by the photodiode detector. As the AFM tip is moved from left to right, up-down deflections in the sample are detected by the photodiode detector and converted into digital topographical images.

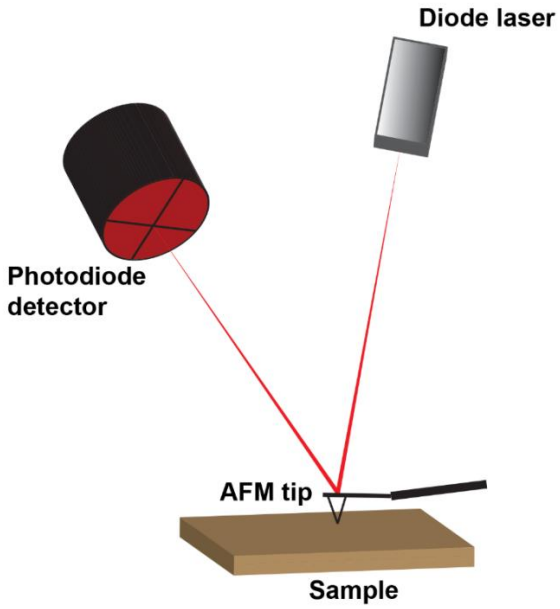

Figure 2: Configuration of instruments in the atomic force microscope. The basic equipment layout is illustrated for the Bruker Dimension Icon AFM using PeakForce quantitative nanomechanical mapping (QNM) mode in air. Up-down bending of the cantilever in response to sample surface topology is recorded by laser deflections to the photodiode detector. Tip model: TAP150A.

All images obtained for length measurements had a scanning area of 20 x 20 μm and were analyzed using ImageJ software as follows: each image scale is set to 680 pixels equal to 20 μm of distance. The scale is set prior to any image modifications. The image is then converted to an 8-bit grayscale, followed by a brightness and contrast (B&C) adjustment in order to better visually separate the grey filaments from the black background. The B&C minimum (12) and maximum (254) values are always kept constant and used for each image. After B&C adjustments, the image is smoothed out using the "smoothing" option in order to better enhance a future skeletonization step. The background is then subtracted using a "rolling ball" algorithm, which corrects for any uneven background illumination. In order to enhance the skeletonization process, a Fast Fourier Transform bandpass filter is applied, this exaggerates the filament outlining, making it easier to quantify. The parameters for the FFT bandpass filter are kept constant for each image. In order to create a binary black and white image, a threshold is applied. The threshold values were optimized using initial automatic program recommendations and those optimal values are then kept constant for each following image. The image is then skeletonized, which makes filaments 1 pixel thick. After skeletonization, the image is closely inspected for filaments that would disrupt the quantification process, such as filaments that are bundled and therefore immeasurable, excluding them from quantifications. The image is also inspected for filaments that are overlapping. Touching filaments would be measured as one long filament, so the two filaments are separated using an eraser tool, erasing at the point of contact. Using the Image J "Analyze Particles" option, filaments are automatically numbered and a list of lengths is generated corresponding to each designated filament number (Fig. 3). Measurements are saved and plotted as histograms charts using Prism (version 5.02).

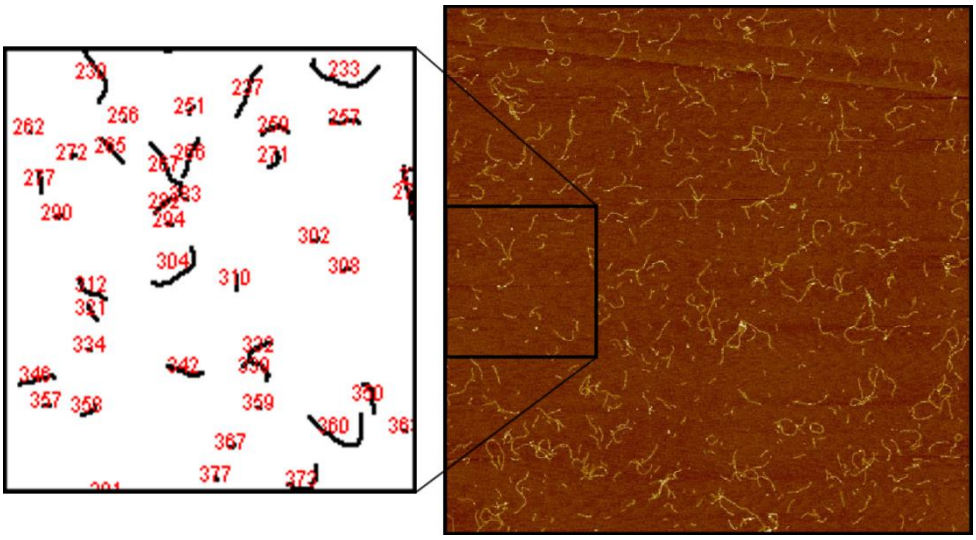

Figure 3: ImageJ filament length acquisition. Skeletonized filaments are analyzed and enumerated as single particles using ImageJ software. The perimeter of particles are used to obtain single length measurements for each sample.

Determination of Young's modulus for desmin filament networks

A force-distance analysis was conducted to obtain a Young's modulus (E) of DIF networks with and without nebulin. All force measurements were obtained using the AFM PeakForce QNM mode in air. PeakForce QNM mode allows us to simultaneously gather sample modulus along with high-resolution topography images. Using the undersurface grid markings previously described, the samples were navigated in search for highly dense areas of filament networks. Once identified, we continuously narrowed our scanning area to ensure that the tip was centered directly over the filament network (Fig. 4). Proper tip placement is important in minimizing the substrate effect caused by the AFM tip coming into contact with the hard mica surface rather than a filament network. The AFM tip, model: TAP150A (Bruker) with a normal spring constant of 5 N/m, was drawn into contact with a highly concentrated area of the protein sample (Fig. 4). Prior to any sample measurements, tip deflection sensitivity was calibrated using a sapphire

sample (Bruker). The tip was then retracted from the dense filament network, obtaining a Young's modulus reading by measuring force relative to tip displacement as shown in Figure 5.

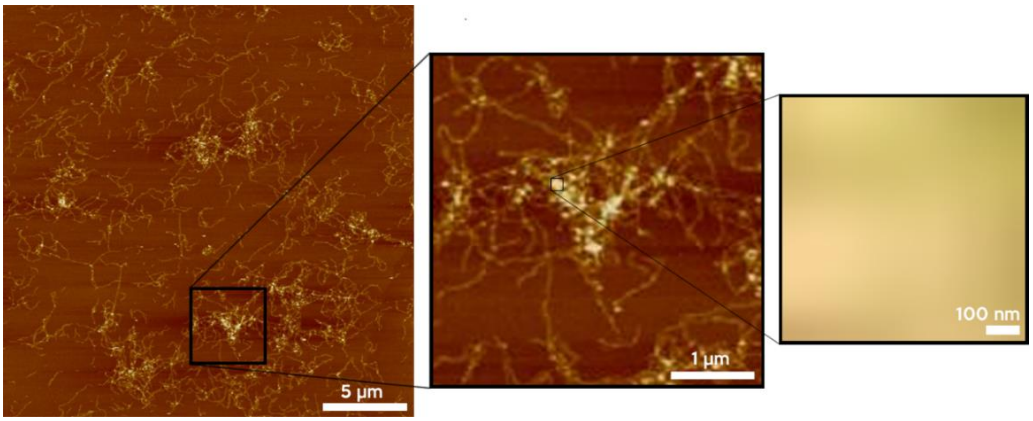

Figure 4: Procedure for determining Young's modules for dense filament networks. The AFM scanning area is progressively decreased to ensure proper tip placement over a dense filament network.

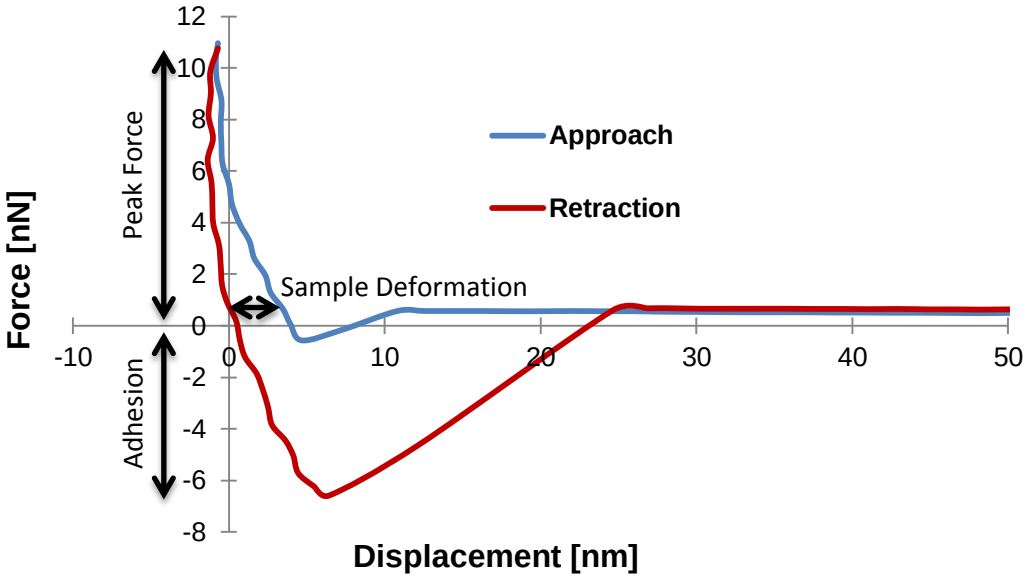

Figure 5: Force-distance analysis of dense filament networks. The AFM tip is drawn into contact (Approach) with a concentrated area of the protein sample. The tip is then retracted from the network (Retraction), generating a Young's modulus reading by measuring force relative to tip displacement.

CHAPTER III

RESULTS

Mutant desmin E245D impairs early desmin assembly by decreasing filament lengths

Intrinsic differences in the initial assembly interactions among desmin WT and its desminopathy-linked mutant, E245D, were found by measuring filament lengths 10 min after the initiation of assembly *in vitro*. Recombinant human desmin WT, its E245D mutant, and an equimolar heterozygous protein mixture were prepared and analyzed using methods described above. To further understand the molecular etiology for desminopathy caused by mutant desmin E245D, human proteins, rather than mouse proteins, were used in this study. Visual examination of high-resolution images of isolated single filaments by atomic force microscopy immediately after deposition on mica grids revealed similarly flexible and smooth filaments for the three samples (Fig. 6 A, B, C). However, more detailed observations revealed that the heterozygous protein samples filaments (WT / E245D) looped more frequently than others, leading to a more twisted rope-like configuration (arrowheads point to loops Fig. 6 C).

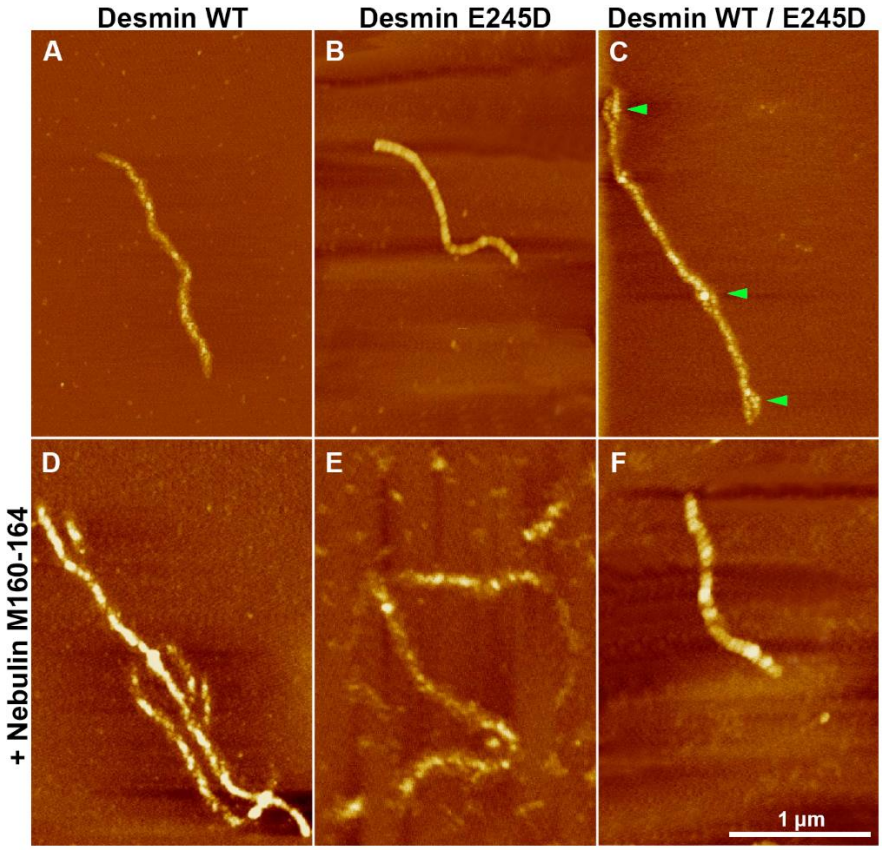

Figure 6: Topology of single desmin filaments with and without nebulin. Panels show: desmin WT (A), mutant desmin E245D (B), and an equimolar heterozygous mixture (C), each with and without muscle actin-binding partner, nebulin (D, E, and F). Arrowheads point to rope-like loops formed by mature filaments (C). Samples were imaged 10 min after the initiation of assembly. Proteins were absorbed onto mica surfaces and imaged with AFM using QNM mode. Final protein concentration on grid: 0.0125 g/L. Mag bar: 1 µm.

The length distribution of several thousands of desmin filaments, measured using a computer-based Java algorithm, revealed that the mutant desmin E245D protein made significantly shorter filaments when compared to WT or heterozygous desmin. Table 1 summarizes the results obtained from the length measurements of single human desmin filaments 10 min after the initiation of assembly in Tris-HCl pH 8.4 buffer system (for more details, refer to Methods section). The average single filament length for the mutant desmin E245D was approximately 30% shorter than that of the desmin WT. Similarly, separate experiments using similar assembly

conditions obtained the same results (Appendix Table 3). A histogram of all the length measurements obtained in our analysis of human proteins shows that the mutant desmin E245D had a higher frequency of shorter filaments within a distribution range of 0.15 to 0.35 µm (Fig. 7). In comparison to desmin WT, the heterozygous mixture (WT / E245D) had no significant difference in length measurements (Table 1). Thus, we conclude from our results that shorter mutant desmin filaments, along with an increased tendency to aggregate, indicates that the desmin E245D mutation negatively affects the filament assembly process. One possibility is that this mutant desmin disrupts filament elongation very early during the assembly process, yielding shorter mature filaments.

Table 1: Length measurements of single desmin filaments

	Mean (µm)	Median (µm)	*SE	¥N	Range (µm)
Des WT	0.686	0.43	0.014	2494	0.08 – 5.05
Des E245D[6]	0.473	0.31	0.008	3172	0.08 – 4.40
WT / E245D	0.627	0.43	0.011	2754	0.08 – 9.76

*SE = Standard Error of Mean

¥N = Number of single filaments measured

Image analyses of large populations of desmin filaments revealed a similar pattern as the one observed with single filaments. Comparison of WT and heterozygous desmin assembled filaments showed evenly distributed filaments with roughly equal grid coverage. However, with this analysis, we consistently noticed an increased aggregate formation for the E245D mutant (aggregates are denoted by asterisks, Fig. 8 B). Specifically, we found an average of two large aggregates per 20 x 20 µm scanning area, approximately 0.25 µm in diameter for mutant desmin (Fig. 8 B, asterisks). This indicates that this mutant desmin is able to form elongated filaments, yet has a propensity to aggregate as compared to desmin WT under nearly identical conditions.

Furthermore, we also noted that the heterozygous sample exhibited smaller scattered aggregates of protein as compared to those observed for mutant desmin but rarely observed for desmin WT.

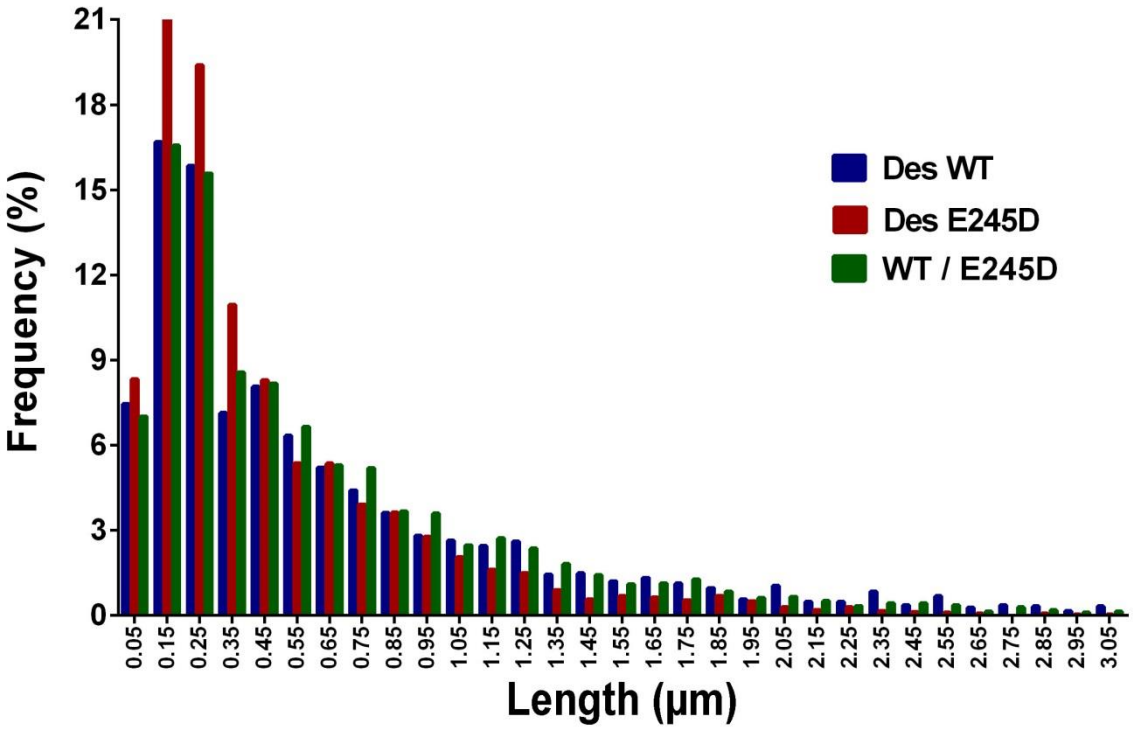

Figure 7: Distributions and comparison of desmin single filament length measurements. Plotted are histograms of the lengths measured using imageJ software for desmin WT (blue, n=2494) mutant desmin E245D (red bars, n=3172) and heterozygous WT / E245D desmin (green bars, n=2754) assembled for 10 min in 150 mM NaCl, Tris-HCl pH 8.4. Data shows that mutant desmin had a higher frequency of shorter filaments, compared to the WT or the heterozygous protein mixture. Notice that the frequency of red bars is higher for shorter lengths and significantly drops for longer lengths, while that for WT or heterozygous desmin remains constant. The histogram was plotted with a bin sample size: 0.1 µm.

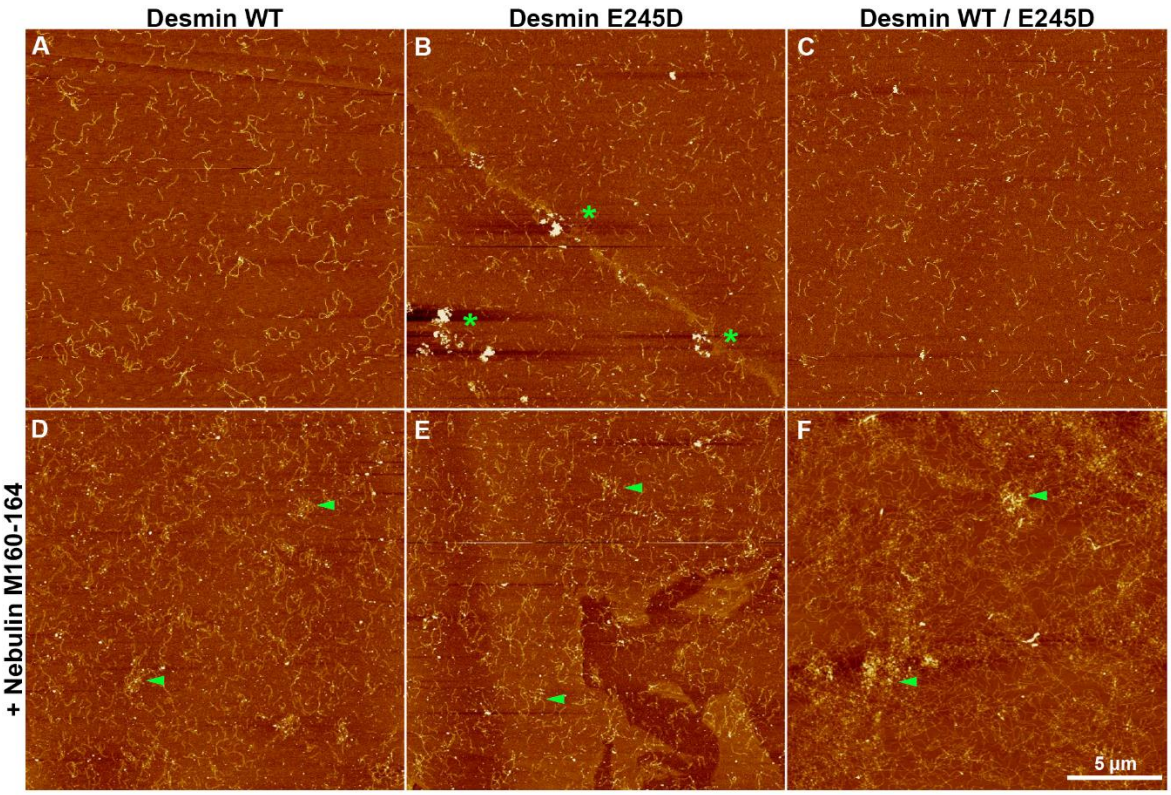

Figure 8: Topological coverage of populations of desmin filaments during early stages of filament assembly, co-assembled with or without nebulin. All AFM images if desmin filaments were obtained 10 min after the initiation of assembly (see Methods for details). Panels show: desmin WT (A), mutant desmin E245D (B), and an equimolar heterozygous mixture (C), each with and without muscle actin-binding partner, nebulin (D, E, and F). Mutant desmin E245D (B) displayed an increased amount aggregate formation (asterisks). Addition of nebulin increased filament localization (D, E, and F). Arrowheads indicate a few specks resembling nebulin (D, E, and F). Samples were imaged 10 min after the initiation of assembly. Proteins were absorbed onto mica surfaces and imaged with AFM using QNM mode. Final protein concentration on grid: 0.0125 g/L. Image size: 20 x 20 µm. Mag bar: 5 µm.

Nebulin M160-164 acts as a desmin intermediate filament coupler-protein

The small uniform white specks dispersed throughout the mica surface are presumed to correspond to nebulin (arrowheads, Fig. 8 D, E, F), since evaluation of this nebulin alone, yielded similar globular rounded structures (see Appendix Fig. 13). Nebulin appears to

consistently increase the clustering of groups of desmin filaments to specific areas on the mica, probably by coupling filaments together into a network (see arrowheads, Fig. 8 D, E, and F). Compared to desmin samples without nebulin (A, B, and C), samples with nebulin (D, E, and F) are less evenly dispersed and showed a higher tendency to clump together. One explanation is that nebulin acts as an IF-specific coupling protein that bundles desmin filaments to impart their directionality. In the context of a living muscle cell, we predict that nebulin integrates actin filaments to the IF cytoskeletal system, by marking the exact spatial locale of thin filaments to the Z-discs, in a highly flexible binding interaction, to align each sarcomere to each other.

Due to the clumping effects exerted by nebulin on desmin filaments, length measurements for single filaments in the presence of nebulin were challenging. The major issue faced was the increased overlap of filaments when co-assembled with nebulin, making it difficult to attain an accurate distinction of each individual filament, a requirement for length measurements (see Fig. 8 panels D, E, and F). Nevertheless, we were able to find lower concentrations of proteins that allowed conditions with adequate filament separation (Appendix Table 3). In this analysis, we found that mutant desmin bound to nebulin had significantly shorter lengths when co-assembled with mutant desmin E245D than with WT desmin. All together, both studies conclusively support the idea that shorter filaments are formed in the early steps of assembly of mutant desmin E245D. This fact could potentially explain, at a nanoscale level, what happens in the muscle sarcomeres of patients bearing this particular desmin mutation. Shorter mutant desmin filaments are predicted to negatively compromise the synchronous cycles of relaxation and contraction by excessively pulling the thin filaments to the Z-discs.

Desmin networks show a decrease in network elasticity in the absence of nebulin M160-164

Differences in network characteristics among desmin WT and its desminopathy-linked mutant desmin E245D, with and without the presence of nebulin, were found by measuring a Young's modulus (E) of highly-concentrated dense desmin filament networks, 10 min after the initiation of assembly *in vitro*. Recombinant desmin WT, mutant desmin E245D, and an equimolar heterozygous protein mixture, were prepared and analyzed using methods described above (see Materials and methods). Table 2 summarizes the results obtained from the force-distance analysis of dense desmin networks. Without nebulin, desmin networks recorded a high Young's modulus, correlating to low network elasticity and high network stiffness (Fig. 9). With a mean difference of less than 2 GPa, desmin networks without nebulin were too similar to confidently say there was any significant difference (Table 2). The slight variations in mutant desmin E245D could possibly be attributed to substrate effects (see Materials and methods). We conclude that, in the absence of nebulin, the mutant desmin E245D, along with the heterozygous protein, had no significant difference in network formation when compared to desmin WT networks.

Table 2: Young's Modulus for desmin networks with or without nebulin

	Mean (GPa)	Mean Diff. (GPa)	Significant	¥N
Des WT	7.87	-	-	102
Des E245D	6.90	0.975[a]	No[c]	101
WT / E245D	6.02	1.851[a]	No[c]	100
Neb M160 - 164	1.40	-	-	102
WT + Neb	0.76	-	-	100
E245D + Neb	5.95	5.195[b]	Yes[d]	102
WT / E245D + Neb	3.61	2.851[b]	Yes[d]	100

[a]Mean Diff. = Mean difference compared to Des WT

[b]Mean Diff. = Mean difference compared to Des WT + Neb

[c] t-test compared to Des WT with 95% confidence P-value > 0.05

[d] t-test compared to Des WT + Neb with 95% confidence P-value < 0.05

[¥]N = Number of force measurements obtained

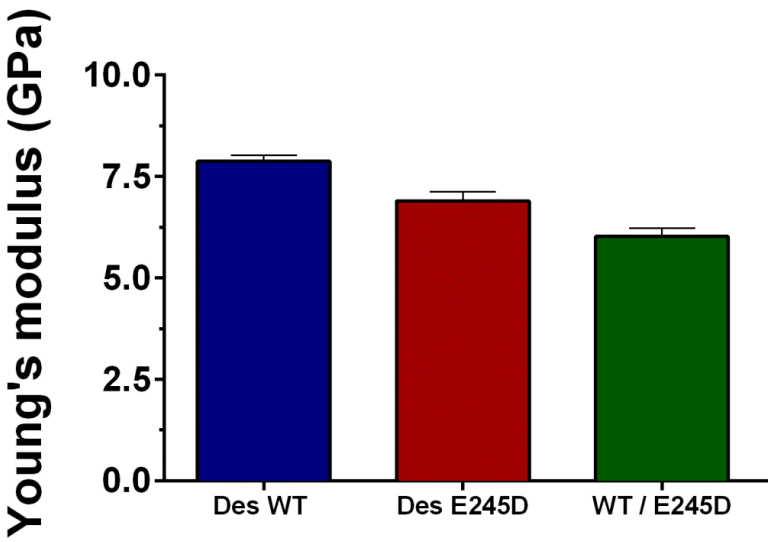

Figure 9: Young's modulus for DIF networks without the addition of nebulin M160-164. A force-distance analysis was conducted to obtain a Young's modulus of desmin intermediate filament networks without nebulin. All readings were obtained using AFM in QNM mode. The AFM tip is drawn into contact with a highly concentrated area of the protein sample, and then immediately retracted from the dense filament network, generating a Young's modulus reading by measuring force relative to tip displacement. Analysis shows high network stiffness and low network elasticity for all three protein samples in the absence of nebulin.

Addition of nebulin M160-164 increases network elasticity for desmin WT networks

With the addition of nebulin, desmin WT networks showed a low Young's modulus, corresponding to a high network elasticity and low network stiffness (Fig. 10). Unlike desmin WT in the presence of nebulin, the mutant desmin E245D showed no increase in network elasticity since the Young's modulus remained high (Fig. 10). Paired t-test comparisons between the mutant desmin E245D and the mutant desmin E245D co-assembled with of nebulin (E245D + Neb) showed no significant difference (P-value > 0.05). Expectedly, the heterozygous protein yielded a value in between, given that this sample is a 1:1 molar ratio of desmin WT to mutant

desmin E245D (Fig. 10). From this analysis, we conclude that the mutant desmin E245D did not appropriately respond to nebulin binding, leading to a significantly inelastic network. Note that the Young's modulus of the mutant E245D plus nebulin is stiffer when compared to WT desmin, while an intermediate response was recorded for the heterozygous sample in response to nebulin.

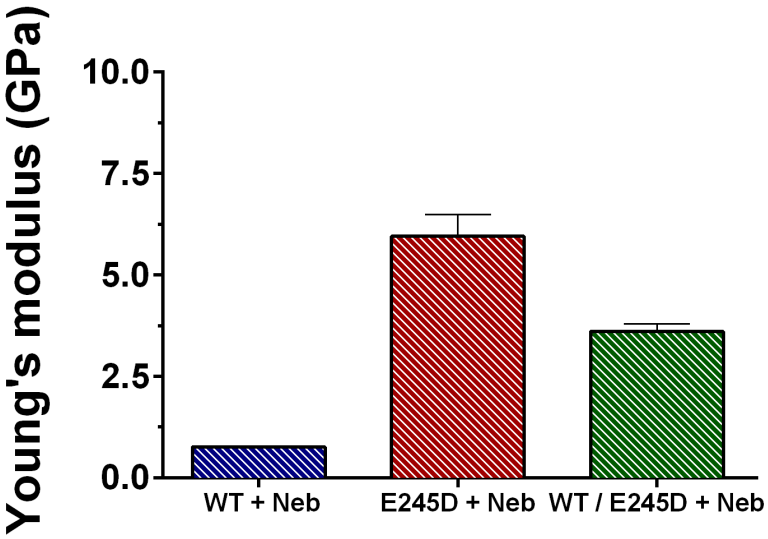

Figure 10: Young's modulus for DIF networks with the addition of nebulin M160-164. A force-distance analysis was conducted to obtain a Young's modulus of desmin intermediate filament networks with the addition of nebulin. All readings were obtained using AFM in QNM mode. The AFM tip is drawn into contact with a highly concentrated area of the protein sample, and then immediately retracted from the dense filament network, generating a Young's modulus reading by measuring force relative to tip displacement. Analysis shows that the addition of nebulin increased network flexibility for WT + Neb, while the E245D + Neb was unaffected, and the heterozygous protein showed characteristics of both.

CHAPTER IV

DISCUSSION

The proper linkage and alignment of myofibrils is essential for force transmission throughout the muscle [5]. By connecting series of myofibrils along their Z-discs to the plasma membrane and nuclear envelope, desmin limits the degree at which myofibrils slide past one another during active muscle contraction and passive relaxation, thereby preventing internal cell damage. By directly binding to nebulin, desmin intermediate filaments provide the structural network required for the normal function of myofibrils. Impairments in the binding between desmin and nebulin are supported by the analysis of nebulin mice knockout skeletal muscles that show misalignment of myofibrils shortly after the pups are born [4, 12]. On the other hand, mutations in desmin yield to muscle weakness and progressive cardiomyopathy in humans, often resulting in cardiac transplants as the sole treatment option [7].

In this study, we report that the mechanical changes brought upon mutant desmin – which is linked to desminopathy – are dependent on its interaction with nebulin, at the filament and network levels *in vitro*. Specifically, this study focused on a class of desmin mutations that does not arrest filament assembly [9], that is, this type of mutant desmins are assembly-competent, yet still cause desminopathy in humans. Thus, the current paradigm is that these types of desmin mutations cause disease by alterations in the mutant proteins binding interactions with binding partners. We chose to study the desmin E245D mutation, not only because it maps in coil 1B, but also because it is the region within desmin reported to have the highest binding affinity to its muscle-binding protein partner, nebulin [13]. This particular desmin mutation interferes with the

ability of nebulin to precisely regulate the lengths of actin filaments in myocytes. This particular desmin mutation has been reported in two separate families and it is associated with restrictive cardiomyopathy, muscular atrophy, and increased risk of sudden cardiac death [6]. Furthermore, studies have attributed the etiology of this particular desmin mutation to defects in the interaction between desmin and nebulin, that are thought to directly mechanically alter the 3D cytoskeletal scaffold and force transmission capabilities of sarcomeres over time [13, 14].

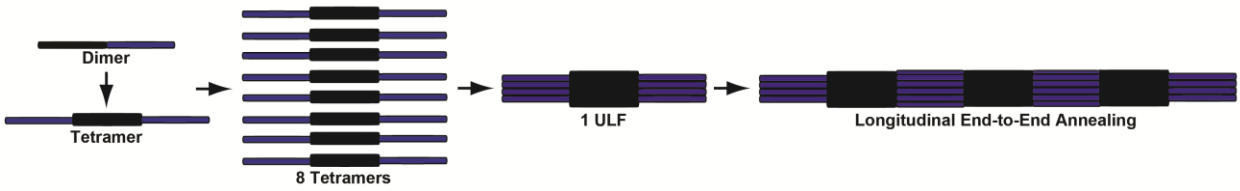

Figure 11: Model for desmin intermediate filament assembly from dimer to mature filament. Desmin filaments are assembled by lateral interactions of staggered desmin dimers that assemble in an antiparallel fashion. A tetramer is formed by dimer-dimer overlap at the coil 1B (black). Further interaction of 8 tetramers results in the formation of 1 unit-length filament (ULF), which anneals longitudinally to other ULFs to form mature elongated filaments. Note: in cells, in addition to the longitudinal annealing mechanism depicted above, there is evidence for another assembly mechanism termed intercalary subunit exchange [15].

Mutant desmin E245D filaments show structural defects prior to nebulin binding

In this study, we obtained single filament length measurements of desmin molecules from two independent experiments using AFM instruments from different manufacturers (Bruker and Nanoscope), yet using similar assembly conditions. Both experiments used human WT and mutant desmin E245D. The measurements obtained are reported in Table 1 and Appendix Table 3. Our findings, in both cases, are that mutant desmin E245D forms significantly shorter filaments when compared to desmin WT under identical assembly conditions. Furthermore, we

report that co-assembly of nebulin with mutant desmin leads to further shortening. Using the length measurements obtained in this study for desmin filaments and referencing them to the known lengths of the average vimentin ULFs of 65 nm [8], we approximated the number of ULFs that assembled end-to-end to form a mature desmin filament (Fig. 12). Because the mutant desmin E245D forms seemingly normal looking filaments as examined by transmission electron microscopy [9], we previously predicted that some molecular phenotypes found in desminopathy patients associated with this particular mutation results from an improper binding interaction between desmin and nebulin. Here, using high-resolution AFM imaging, we determined that the lengths of these mutant desmin filaments were indeed decreased at the early stages of filament assembly, even before nebulin was added. Furthermore, we report the finding that the decrease in length of this mutant desmin is sustained upon nebulin binding (Appendix Table 3).

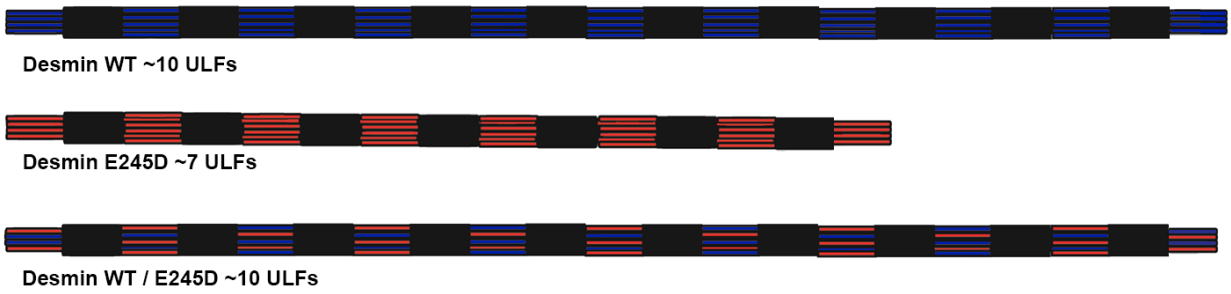

Figure 12: Model for the early assembly of 'assembly competent' mutant desmin linked to desminopathy. The model depicts color-coded desmin filaments 10 min after the initiation of assembly: WT (blue), E245D (red), heterozygous WT / E245D (mixed). The filament lengths are based on the mean length determined by AFM measurements (Table 1), and are expressed using the known lengths for vimentin ULFs (65 nm).

In the presence of nebulin, desmin WT filaments lengthened while mutant desmin E245D filaments shortened when compared to the same proteins without nebulin (Appendix Table 3).

Note that in these studies, to measure filament lengths in the presence of nebulin more accurately, proteins were used at a lower concentration, this allows for a greater spread and minimizes the clumping affects elicited by nebulin. At higher filament density, as noted in the results section, it was challenging to determine filament lengths due to the tendency of nebulin to clump desmin (Fig. 8 D, E, F).

Mutant desmin E245D bound to nebulin impedes network flexibility

To determine if the mutant desmin had different mechanical properties at a network level that could help explain the clinical symptoms of patients bearing the desmin E245D mutation, we decided to determine the mutant desmin networks force-bearing properties. For this purpose, a force-distance analysis was generated to acquire an elastic modulus of dense desmin filament networks with and without the presence of nebulin. Because desmin is a cytoskeletal protein primarily responsible for the structural stability and proper alignment of actively moving myofibrils, we proposed that exploring the desmin networks elastic properties was essential to gaining a better understanding of desminopathies.

In the absence of nebulin, all desmin networks showed limited flexibility, generating a relatively high Young's modulus of up to 6 GPa (Fig. 9 and Table 2). Similar studies using AFM by other groups were used to analyze the mechanical properties of single filaments of vimentin, another IF protein very similar in size and structure to desmin. That study reported vimentin Young's modulus of approximately 0.9 GPa [16]. While the values we obtained in our study were much higher, we can attribute these differences to the fact that we measured a dense filament network, while the values that were reported in the study were measured for single vimentin filaments.

We also found that, in the presence of nebulin, desmin WT networks generated a low Young's modulus of around 0.76 GPa, suggesting that, when desmin binds to nebulin, it becomes very flexible (Fig. 10). This is expected, as the sarcomere in cardiac muscle repeatedly contracts and relaxes during the lifetime of a human. A dynamic and flexible network of cytoskeletal proteins is required to maintain proper muscle function in response to physiological stimuli. Unlike the networks for desmin WT, the mutant desmin E245D networks were stiffer. Under the conditions used in our study, we measured none or little response in network flexibility upon the addition of nebulin (Fig. 10 and Table 2). Filament networks for the mutant desmin E245D remained stiff and inelastic compared to desmin WT under similar conditions. Consequently, we predict that the increased network stiffness, observed with the mutant desmin E245D networks, potentially contribute to serious deleterious consequences for patients. By losing IF flexibility due to its inability to bind nebulin, the stiff mutant desmin network loses its dynamic ability of keeping up with repeated myofibril contractions, therefore, decreases its efficiency at maintaining structural stability and alignment, while increasing the likelihood for damage. In conclusion, based on our findings we propose that our results, in fact, offer a new mechanism for how the mechanical properties of the desmin network is compromised in desminopathy caused by the desmin E245D mutations inability to properly bind nebulin in humans.

REFERENCES

1. Omary, M.B., "IF-pathies": a broad spectrum of intermediate filament-associated diseases. Journal of Clinical Investigation, 2009. 119(7): p. 1756-1762.

2. Lazarides, E. and B.D. Hubbard, Immunological characterization of the subunit of the 100 A filaments from muscle cells. Proc Natl Acad Sci U S A, 1976. 73(12): p. 4344-8.

3. Conover, G.M. and C.C. Gregorio, The desmin coil 1B mutation K190A impairs nebulin Z-disc assembly and destabilizes actin thin filaments. J Cell Sci, 2011. 124(Pt 20): p. 3464-76.

4. Tonino, P., et al., Reduced myofibrillar connectivity and increased Z-disk width in nebulin-deficient skeletal muscle. J Cell Sci, 2010. 123(Pt 3): p. 384-91.

5. Shah, S.B., et al., Structural and functional roles of desmin in mouse skeletal muscle during passive deformation. Biophys J, 2004. 86(5): p. 2993-3008.

6. Vrabie, A., et al., The enlarging spectrum of desminopathies: new morphological findings, eastward geographic spread, novel exon 3 desmin mutation. Acta Neuropathol, 2005. 109(4): p. 411-7.

7. Goldfarb, L.G., et al., Intermediate filament diseases: desminopathy. Adv Exp Med Biol, 2008. 642: p. 131-64.

8. Herrmann, H., et al., Characterization of distinct early assembly units of different intermediate filament proteins. J Mol Biol, 1999. 286(5): p. 1403-20.

9. Bar, H., et al., Severe muscle disease-causing desmin mutations interfere with in vitro filament assembly at distinct stages. Proc Natl Acad Sci U S A, 2005. 102(42): p. 15099-104.

10. Goebel, H.H., Congenital myopathies at their molecular dawning. Muscle & Nerve, 2003. 27(5): p. 527-548.

11. Herrmann, H., L. Kreplak, and U. Aebi, Isolation, characterization, and in vitro assembly of intermediate filaments. Methods Cell Biol, 2004. 78: p. 3-24.

12. Bang, M.L., et al., Nebulin-deficient mice exhibit shorter thin filament lengths and reduced contractile function in skeletal muscle. J Cell Biol, 2006. 173(6): p. 905-16.

13. Conover, G.M., S.N. Henderson, and C.C. Gregorio, A myopathy-linked desmin mutation perturbs striated muscle actin filament architecture. Mol Biol Cell, 2009. 20(3): p. 834-45.

14. Baker, L.K., et al., Nebulin binding impedes mutant desmin filament assembly. Mol Biol Cell, 2013. 24(12): p. 1918-32.

15. Colakoglu, G. and A. Brown, Intermediate filaments exchange subunits along their length and elongate by end-to-end annealing. J Cell Biol, 2009. 185(5): p. 769-77.

16. Guzman, C., et al., Exploring the mechanical properties of single vimentin intermediate filaments by atomic force microscopy. J Mol Biol, 2006. 360(3): p. 623-30.

APPENDIX

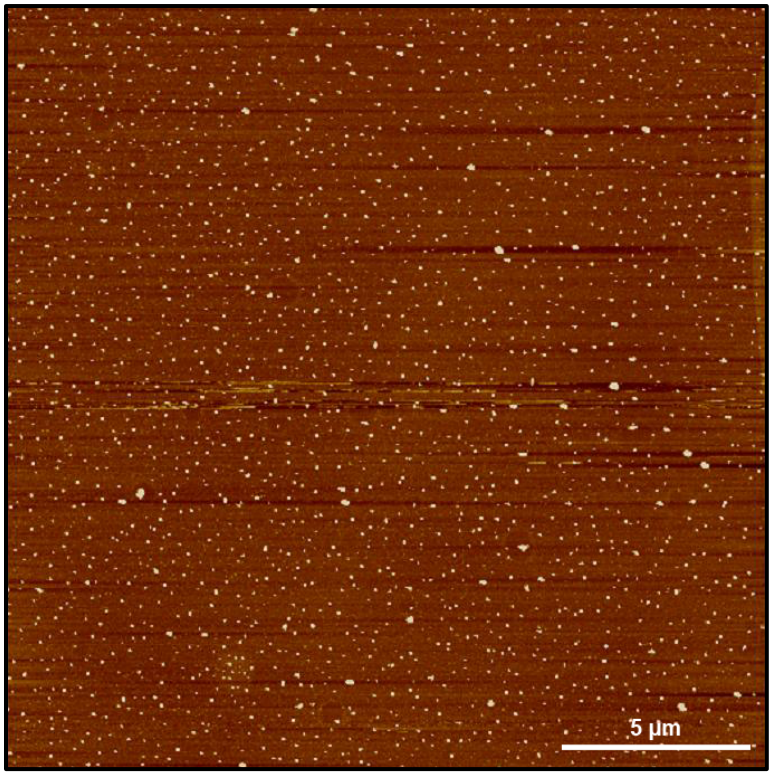

Figure 13: Topological coverage of nebulin M160-164. Nebulin M160-164 was imaged and prepared under the same assembly conditions as described for desmin (see Methods for details). After 10 min at 37°C, the nebulin fragment was absorbed onto a mica surface and imaged with AFM using QNM mode. Final protein concentration on the grid: 0.0125 g/L. Image size: 20 x 20 µm. Mag bar: 5 µm.

Table 3: Length measurements of single desmin filaments with or without nebulin

	Mean (µm)	Median (µm)	*N
Des WT	0.666	0.52	693
Des E245D	0.519	0.33	866
Des WT + Neb	0.753	0.57	526
E245D + Neb	0.435	0.32	2086

Proteins were assembled for 10 min at 37°C in 100 mM NaCl, 5 mM Tris-HCl, pH 8.4.

Analyzed using AFM (Nanoscope).

*N = Number of single filaments measured